

Biomass-Gas-and-Nuclear-To-Liquids (BGNTL) Processes Part I: Model Development and Simulation

Authors:

James Alexander Scott, Thomas Alan Adams II

Date Submitted: 2018-08-07

Keywords: Polygeneration, Synthetic Fuels, Nuclear, Natural Gas, Biomass

Abstract:

New polygeneration processes for the co-production of liquid fuels (Fischer-Tropsch liquids, methanol, and dimethyl ether) and electricity are presented. The processes use a combination of biomass, natural gas, and nuclear energy as primary energy feeds. Chemical process models were created and used to simulate candidate versions of the process, using combinations of models ranging from complex multi-scale models to standard process flowsheet models. The simulation results are presented for an Ontario, Canada case study to obtain key metrics such as efficiency and product conversions. Sample Aspen Plus files are provided in the supplementary material to be used by others.

Record Type: Preprint

Submitted To: LAPSE (Living Archive for Process Systems Engineering)

Citation (overall record, always the latest version):

LAPSE:2018.0393

Citation (this specific file, latest version):

LAPSE:2018.0393-1

Citation (this specific file, this version):

LAPSE:2018.0393-1v1

DOI of Published Version: <https://doi.org/10.1002/cjce.23231>

License: Creative Commons Attribution-NonCommercial-NoDerivatives 4.0 International (CC BY-NC-ND 4.0)

Biomass-Gas-and-Nuclear-To-Liquids (BGNTL) Processes

Part I: Model Development and Simulation

J. Alexander Scott and Thomas A. Adams II*

Department of Chemical Engineering, McMaster University

1280 Main St. West, Hamilton, ON, Canada

Corresponding Author Contact: tadams@mcmaster.ca

Keywords: Biomass, Natural Gas, Nuclear Energy, Synthetic Fuels, Methanol, Dimethyl Ether, Energy Conversion, Polygeneration

ABSTRACT

New polygeneration processes for the co-production of liquid fuels (Fischer-Tropsch liquids, methanol, and dimethyl ether) and electricity are presented. The processes use a combination of biomass, natural gas, and nuclear energy as primary energy feeds. Chemical process models were created and used to simulate many candidate version of the process, using a combinations of models ranging from complex multi-scale models to standard process flowsheet models. The simulation results are presented for an Ontario, Canada case study to obtain key metrics such as efficiency and product conversions. A sample Aspen Plus file is provided in the supplementary material to be used by others.

1. INTRODUCTION

The government of the province of Ontario, Canada, has made a commitment to decarbonizing its energy infrastructure.^[1] For example, all bulk electricity production from coal in the province has ceased, and the Atikokan generating station was converted from a coal-fired to a wood-pellet-fired thermal power plant at 205MW (the largest of its kind in North America).^[2] Ontario also has a cap-and-trade style carbon market,^[3] with the Federal government setting a carbon tax floor (which increases annually) in case the provincial system does not result in high enough carbon prices.^[4] In addition, Ontario's electricity grid makes heavy use of nuclear, hydropower, and non-

hydropower renewable resources (wind and solar) consisting of about 58.5%, 23.3%, and 9.5% of the total power produced, respectively. Fossil-fuels (primarily natural gas) in Ontario account for only 8.2% of the electricity generation mix,^[5] which is primarily used for peaking. As a result, less than 4% of Ontario's greenhouse gas (GHG) emissions arise from electricity generation.^[6] Because so few fossil fuels are used to produce electricity, and because there is potentially an oversupply of baseload electricity at present,^[2] the carbon dioxide reductions that can be achieved by further decarbonisation efforts in the electricity sector is relatively small. For these reasons among others, the province has decided not to construct new nuclear units for electricity purposes.^[2] However, there is much room for improvement in Ontario's transportation-related emissions, which are about 58.7 Mt_{CO2e}/yr and account for almost 35% of its total emissions.^[6]

Canada has a particularly large supply of biomass in commercial production (roughly 143 Mt/yr, including agriculture).^[7] In 2014, 1.8Mt/yr of this in the form of wood pellets (a particularly useful form of non-food-competitive energy biomass), 90% of which was exported (primarily to Europe) to be used as a biofuel there, with wood pellet exports growing quickly.^[8] Ontario has the majority share of wood pellet production capacity, at about 1Mt/yr, with the potential for additional growth in capacity in eastern Ontario^[9] and southeastern Ontario to a lesser extent,^[8] particularly in regions hardest-hit by pulp-and-paper industry declines. From a big picture perspective, it makes sense to consume more Ontario-grown biomass locally for bioenergy purposes rather than consuming it in Europe, since the negative environmental impact of trans-Atlantic shipping is by no means negligible. Therefore, by both diverting existing wood pellet production toward biofuel production in Ontario and increasing pellet production capacity for the same, it should be possible to reduce GHG emissions for both Ontario and the world, even accounting for the reduced biomass availability in Europe.

However, Ontario has another underutilized low-carbon energy resource: nuclear energy. Ontario has a long history of safely operating nuclear energy, the necessary technology expertise, the necessary regulatory infrastructure, a supply chain of domestic uranium which currently produces 22% of the world supply,^[10] and a voting public that continues to accept nuclear power as the primary electricity driver in their province (though perhaps not in their own back yards). However, although the next generation (Gen IV) of Canadian nuclear technology is in development (the

Super Critical Water Reactor CanDU Design, or SCWR CanDU),^[11] it has little prospect for use for electricity generation within Ontario in the near future. However, it has significant potential for use in fuel production, such as for the production of hydrogen^[12] or for syngas^[13] which can be used to make synthetic gasoline, diesel^[14], and dimethyl ether (DME, a diesel substitute).^[15] Since nuclear plants that produce fuels and not electricity do not have major issues associated with electricity transmission losses, they do not need to be located close to metropolitan areas which can help alleviate public anxiety about nuclear plant proximity.

Therefore, we present the first biomass-gas-and-nuclear-to-liquids (BGTNL) polygeneration plant design available in the open literature to the best of our knowledge. We considered natural gas as a potential energy source both because it is readily accessible in Ontario, and because previous studies have shown that it is often preferable to use a combination of a fuel that produces hydrogen-rich syngas (e.g. natural gas) and a solid fuel that produces hydrogen-lean syngas (e.g. coal or biomass), rather than the coal/biomass alone,^[16] particularly in the context of polygeneration.^[17] We used chemical process modeling techniques to compute the necessary mass and energy balance flows and present them in this paper for a base case suitable for use in Ontario. We also provide, for the first time, an Aspen Plus v10 flowsheet containing the converged models as supplementary material¹.

2. PROCESS AND SIMULATION METHODOLOGY

2.1 Process Overview

An outline of the proposed BGNTL process superstructure is shown in Figure 1, and specific details of each step can be found in later subsections. The process begins with biomass crushing and feeding to the gasifier. The woody biomass, CO₂, steam, and high purity O₂ (created in an air separation unit, or ASU) are fed to a downward entrained-flow gasifier to facilitate syngas production. Partial oxidation then occurs in the gasifier, and the raw syngas produced is cooled by one of two means: (1) by raising steam in a radiant steam cooler, or (2) by an integrated reformer (IR), which is composed of an integrated steam methane reformer (SMR) and radiant

¹ Because of journal file size limitations, the simulation files have been deposited into the simulation repository at PSEcommunity.org. The supplementary materials file contains links to those files.

syngas cooler (RSC) with a similar design to that proposed by Ghouse et al.^[18] In that case, the IR utilizes the heat from the raw syngas to reform a stream of natural gas into hydrogen-rich syngas, while the hydrogen-lean biomass-derived syngas leaving the gasifier is cooled. The two syngas streams are unmixed and processed separately downstream. The biomass-derived syngas is quenched using process water to around 200°C.

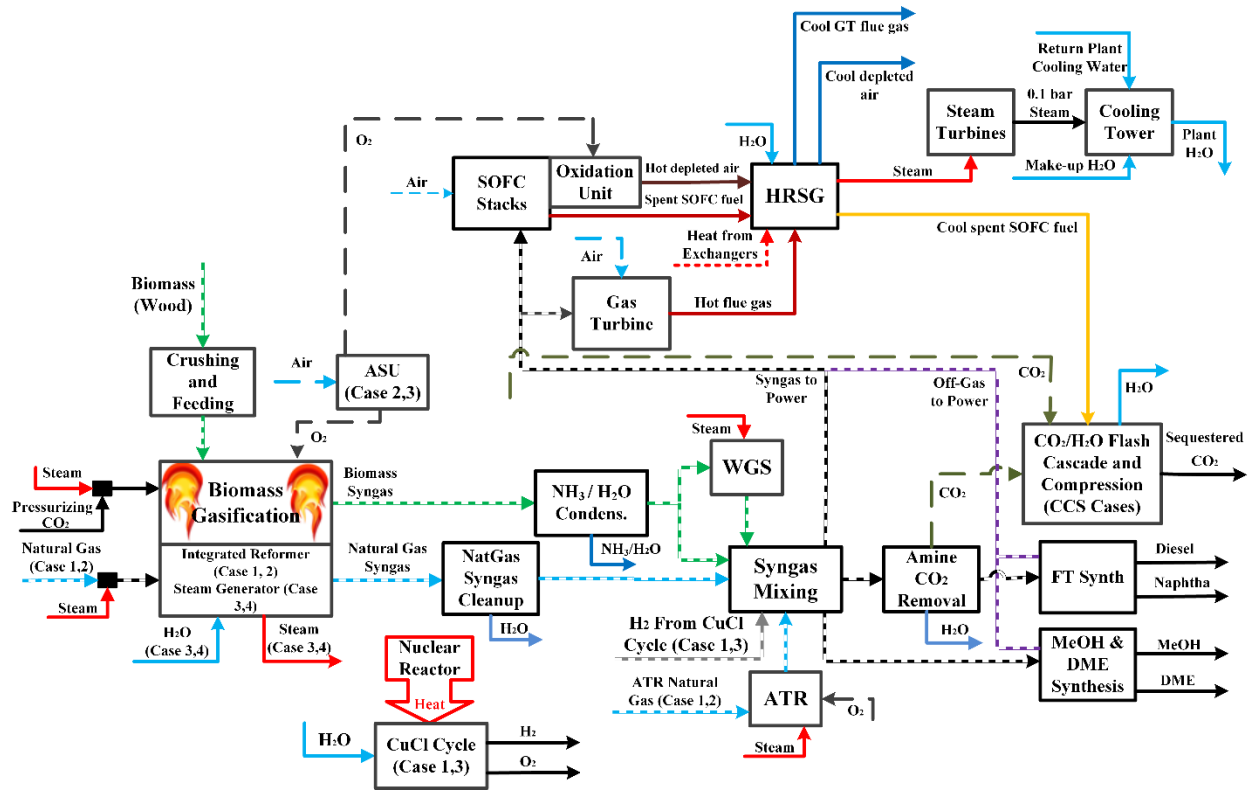


Figure 1. The BGNTL process superstructure used in this work.

The biomass-derived syngas does not need desulfurization because the sulfur content in the wood is so low, resulting in a sulfur content in the syngas of only about 50 ppm. Therefore, water (along with ammonia) can be directly condensed out of the biomass syngas. After this section, the syngas is mixed with gas-derived syngas from the RSC, as well potentially other streams such as syngas coming from an autothermal reformer (ATR), nuclear-derived H₂ from a CuCl cycle, or shifted syngas from a water gas shift (WGS) reactor, depending on the case considered and the optimization results.

After syngas mixing, it is destined for one of three places. It is either mixed to 2.01 H₂/CO molar ratio and sent to either the MeOH/DME section or the FT section, or it is mixed in a non-specific H₂/CO ratio and sent to the power generation system (an amine-based CO₂ removal system is used prior to liquid fuel synthesis). The power generation system consists of either a gas turbine (GT) or a solid oxide fuel cell (SOFC) system for power generation. The power generation system includes a heat recovery and steam generation (HRSG) section for process steam needs and a bottoming cycle for additional electricity production from waste heat. An optional CO₂ purification and compression system is used to prepare captured CO₂ for pipeline transport for either sale or sequestration.

In this work, we considered two different design structures as shown in Table 1. Although the results for both cases will be shown in summarized form, detailed stream and unit operation results for only Case 1.1 will be shown in this work since it demonstrates all aspects of the model conveniently. A future work will examine these cases in an optimization context.

Table 1. Process cases considered in this work.

<i>Case</i>	<i>Case Name</i>	<i>Woody Biomass Used</i>	<i>Natural Gas Used</i>	<i>Nuclear Energy Used</i>	<i>Biomass- syngas cooling method</i>	<i>CCS Used</i>
1.1	BGNTL-CCS-IR	YES	YES	YES	Int. Reforming	YES
1.2	BGNTL-CCS-SteamRSC	YES	YES	YES	Steam Gen	YES

2.2 Simulation Strategy and Basis of Comparison

Both cases shown in Table 1 were modeled utilizing a variety of process simulation tools in combination, including Aspen Plus v10, Matlab, ProMax and gProms, as described in detail in later subsections. ProMax simulations were used for the sulfur and CO₂ absorption sections, which used their proprietary TSWEET physical property package. gProms simulations were used for the integrated reformer, and used various physical property models and correlations which were validated in prior work against experimental data as described in prior work.^[18] All other process section simulations were performed in Aspen Plus using the Peng-Robinson equation of state with the Boston-Mathias modification (PR-BM) property package, except for pure water streams which

used the NBC/NRC steam tables, for flash calculations concerning CO₂ and water phase equilibria at high pressures which used the predictive Soave-Reidlich-Kwong package (PSRK) since prior work showed it to be more accurate than PR-BM under those conditions,^[19] and for the DME/methanol separation sections which used NRTL-RK. Matlab was used as a linking tool to facilitate automation and information transfer between the different software packages.

For a consistent basis-of-comparison in this example, the wood feed rate was fixed at 100 tonne/hr, the nuclear heat input was fixed at 117 MW, and the natural gas rate to the autothermal reformer was fixed at 664 MW_{HHV} for both cases, noting that the ratios of these energy feeds are subject to optimization. However, Case 1.1 contains an additional 169 MW_{HHV} of natural gas feed to the integrated reformer unit in the RSC (determined by the amount of heat available in the RSC), whereas Case 1.2 instead uses boiler feed water to make steam for electricity in the RSC. Each plant was designed such that all utility needs were produced on site, with no utilities imported, with the exception of water. The properties of the primary raw materials used in this work are shown in Table 2.

Table 2. Feedstock properties used in this work.

Biomass Properties			
<i>Ontario Cedar Wood Chips, As Received</i>		<i>Proximate Analysis (wt%)^[20]</i>	
HHV ^[20] (kJ/kg)	19804.82	Fixed Carbon	58.16
LHV ^[20] (kJ/kg)	18790	Volatile Matter	39.94
Average MW of Ash ^[21]	65.15	Ash	1.90
Mole frac Fe ₂ O ₃ in ash ^[21]	0.02613	Moisture	8.00
		<i>Ultimate (wt% dry)^[20]</i>	
		Carbon	48.62
		Hydrogen	5.991
		Nitrogen	0.478
		Sulfur	0.005
		Oxygen	43.006
		Chlorine	0.209
Natural Gas Properties			
<i>Conditions at plant gate</i>		<i>Mole Fractions at Plant Gate ^[14]</i>	
Temperature (°C)	30	Methane	0.939
Pressure (bar)	30	Ethane	0.032
		Propane	0.007
		n-Butane	0.004
		CO ₂	0.010
		N ₂	0.008

The mechanical equipment models used in this work (gas turbines, steam turbines, etc.) used the assumed parameters as shown in Table 3.

Table 3: Assumed efficiencies for mechanical unit operations in the Aspen Plus models used in this work.

Unit Operation	Isentropic Efficiency	Polytropic Efficiency	Mechanical Efficiency	Reference
Compressors		0.85	0.94	[24]
Gas Turbines	0.898		0.988	[15]
Expanders	0.898		0.988	[15]
Steam Turbines	0.875		0.983	[15]
Pumps			0.80	[15]

2.3 Biomass Processing and Gasification Section

The as-received wood chips are first crushed to a maximum particle diameter of 1mm, to achieve optimal mixing while gasifying.^[22] Therefore, a crushing power of 0.02 kWe per kWthHHV of wood was assumed to crush the biomass to the required size.^[22] The crushing itself was not modelled.

The modeled gasifier was a biomass, steam, pressurizing CO₂ and oxygen fed entrained flow gasifier. The system was modeled as a 0-D system in Aspen Plus, which considered the three stages of the gasifier: biomass decomposition, gasification and cooling. The model strategy of Field and Brasington^[23] and of Adams and Barton^[19] (both developed for coal gasification) was adapted for pulverized wood chips by changing the feed properties accordingly. For brevity, the reader is referred to the latter work for a detailed description of the model. In short, the overall approach was to first model the decomposition of biomass into a multi-phase mixture of solid C, solid S, water, H₂ and Cl₂ gases. Then, the gasifier output is estimated by assuming chemical equilibrium at 45 bar and 1300°C of the reaction of decomposed biomass with O₂, high pressure steam (HPS) fed at a rate of 2.8% of the biomass mass flow rate^[24] and pressurizing CO₂ at a rate of 12% of the biomass mass flow rate^[24]. The effects of the low levels of ash that exist in biomass and the need for ash recycle is neglected in this work^[24]. The O₂ flow rate was set such that the temperature of the gasifier was 1300°C. It is also assumed that there is 100% carbon conversion of the gasified biomass and that 2.7% of the heat generated by the gasifier is lost to the surroundings.^[24]

Two different RSC approaches were considered (see Table 1), one with an IR and one with only a steam generator, shown in Figure 2 below. The classic steam generation version uses a simple

heat exchanger model in Aspen Plus that computes the cooling duty necessary to achieve a syngas output temperature of 780°C, and computes the rate of boiler feed water at 101°C and 52 bar necessary to achieve it such that HPS is created at 500°C.

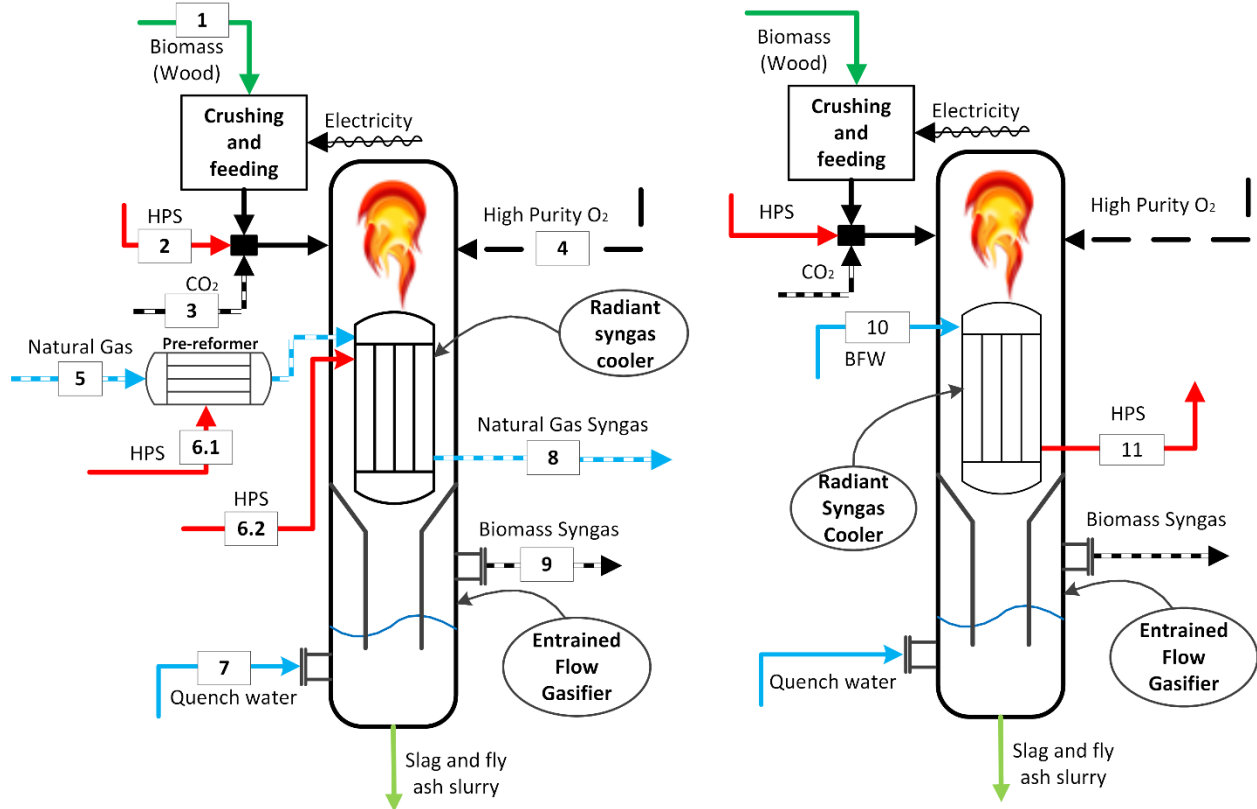


Figure 2. The two radiant syngas cooling options considered in this work. LEFT: Integrated radiant syngas cooling with steam methane reforming. RIGHT: Classic steam generation only.

The model of the IR was based on the design and multi-scale model developed by Ghouse and Adams^[18] for a SMR within the RSC of a coal-fed entrained flow gasifier. For brevity, the reader is referred to Ghouse and Adams^[25] and Ghouse et al.^[18] for full details, and the design and the model is instead summarized here. The reformer consists of two concentric circular rings of vertical tubes inside the shell of the radiant syngas cooler, offset from each other to maximize lines-of-sight to best facilitate radiant heat transfer. The gasifier syngas exhaust flows downward on the shell side of the RSC, and the shell is lined with refractory to prevent heat loss. Each tube is packed with SMR catalyst, with the steam and pre-reformed natural gas feed at the top of the tubes, thus operating in co-current flow (which helps with heat management issues). The gasifier section

contains a neck that allows solids and slag to fall through the middle of the tube rings to minimize contact with the tubes.

The pre-reformer shown in Figure 2 (left) was modelled in Aspen Plus using an REQUIL block at 34.4 bar and adiabatic conditions using the same approach described in Adams and Barton.^[26] The steam flow is sufficiently large and hot enough to reform the higher hydrocarbons adiabatically, but not the methane.^[26] Therefore, the pre-reformer model assumes 100% conversion of the ethane, propane, and butane steam reforming reactions, and assumes chemical equilibrium of the water gas shift and steam methane reforming reactions which have relatively little conversion. The relatively high steam to carbon ratio in the reaction mixture ensures no carbon deposition.^[26]

The model of the IR portion is non-linear, two-dimensional, heterogeneous, and considers axial variations in temperature and composition in the shell and tube gas phases on the dm scale, axial and radial temperature differences in the tube walls on the cm scale, and temperature and composition variations in the catalyst particles on the mm scale. The model considers radiative and convective heat transfer between the shell and tube walls, homogeneous reaction on the shell side (such as water gas shift at high temperatures), conduction within the tube walls, convection within the tube side gases, reaction and diffusion within the catalyst particles, conduction through the refractory walls, and heat losses to the atmosphere. The model used in this work was modified from the original model of Ghouse et al.^[18] by changing the syngas feed composition to match the biomass-derived syngas as predicted from the Aspen Plus gasifier model described above, but otherwise was unchanged. The design parameters chosen for the IR portion were 137 reforming tubes each 20 meters in length and 8 cm in diameter inside of a 4.5 m diameter shell. These were manually selected to work well with a gasifier consuming 100 t/hr of biomass feed, balancing the tradeoffs between cooling duty, methane conversion, and pressure drop. The model was implemented as a set of roughly 100,000 partial differential algebraic equations into gProms and was solved using a finite difference method. Although the model is dynamic, only steady state solutions were used in this work.

Although the design of the IR was fixed, the flow rates of the natural gas and reforming steam were allowed to vary from case to case based on system-wide optimization. Because the gProms model had convergence times that were too long (about an hour per run) to be included in an optimization loop, we created a reduced order steady-state model (ROSSM) from the rigorous gProms model that could be rapidly used within Aspen Plus during optimization without the need to call gProms. To describe briefly, we performed 80 simulation runs using Latin hypercube sampling within a bounded state space of two independent variables, with 60 runs as training data and the rest as testing data. We examined several candidate polynomial (linear-in-the-parameters) models for each of the dependent variables of interest and found that 1st order (linear) models did not represent the nonlinearities well, the 2nd order models that had excellent R² values for both training and testing sets, and that 3rd order models introduced some spurious curvature and so were rejected. The final models ROSSMs used selected for work have the following structure:

$$Z_i = a_{1,i} + a_{2,i} \frac{F_{NG}}{\overline{F_{NG}}} + a_{3,i} \frac{R_{S:C}}{\overline{R_{S:C}}} + a_{4,i} \left(\frac{F_{NG}}{\overline{F_{NG}}} \right)^2 + a_{5,i} \left(\frac{R_{S:C}}{\overline{R_{S:C}}} \right)^2 + a_{6,i} \left(\frac{F_{NG}}{\overline{F_{NG}}} \right) \left(\frac{R_{S:C}}{\overline{R_{S:C}}} \right) \quad (\text{eq 1})$$

where Z_i are the model outputs for variable i as shown in Table A1 in the appendix, $a_{j,i}$ are the model coefficients for coefficient j for output variable i as shown in Table A1. F_{NG} is the flow rate of natural gas in kmol/hr, $R_{S:C}$ is the steam-to-carbon ratio (the molar flow rate of steam divided by the molar flow rate of methane), and $\overline{F_{NG}}$ and $\overline{R_{S:C}}$ are normalization factors (the average of the range of independent variables used in identifying the model). The model was implemented in Aspen Plus using a Calculator block in combination with an RSTOIC model of the reforming equations. The ROSSM model equations were solved analytically by fixing two degrees of freedom: the methane conversion at 80% (a conservative value for SMR),^[18] and the cooling duty at the value required to cool biomass-derived syngas from the gasifier to 780°C. Although it would be preferable to allow these variables to be subject to optimization, we found it necessary to fix them to arrive at manageable optimization times.

An overview of the IR section model as implemented in Aspen Plus is shown in Figure 3.

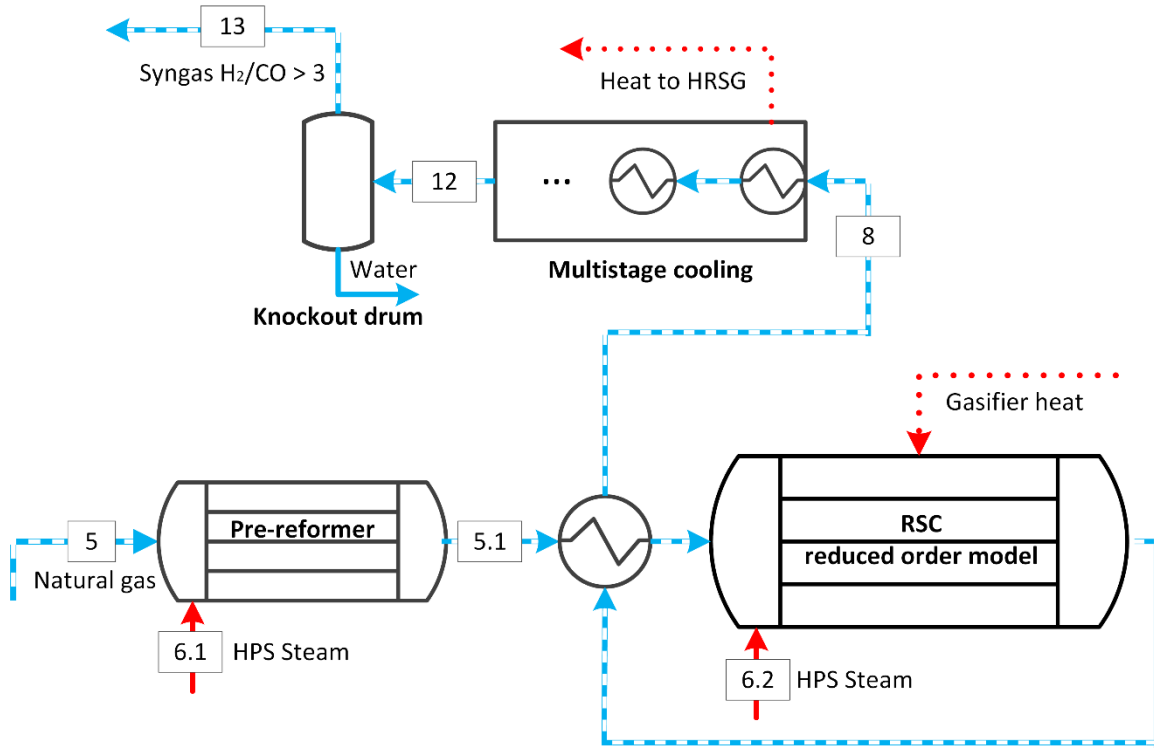


Figure 3. The IR section as modelled in Aspen Plus.

2.4 Air Separation Unit

The air separation unit (ASU) is not directly modeled in this study. However, the power consumption associated with producing O₂ along with a corresponding stream of waste N₂ was considered using the results reported by Clausen et al.,^[24] such as 1 MWe consumed in the ASU per 1 kg/s of O₂ produced at 1 bar. When further compressing the O₂ to 12.9 bar with two stage compression and intercooling (as modelled in Aspen Plus), the total power required becomes 1.333 MWe per 1 kg/s of O₂ produced at 12.9 bar.

2.5 Ammonia Removal

After the gasifier, the biomass-derived syngas is cooled to about 40°C such that most of the water is condensed out, carrying trace ammonia contained in the syngas with it. The remaining syngas is sent to the syngas mixing section. This is modeled with a FLASH2 block in Aspen Plus using the PR-BM equation of state, and shown in Figure 4. Although the cleaning of the recovered sour water is not included in the model, it will be included in the economic analysis in Part II of this work.

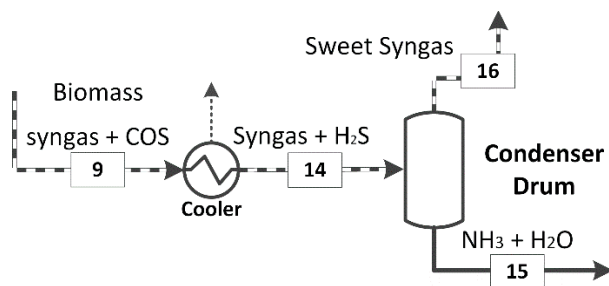


Figure 4. The Ammonia Removal section as modelled in Aspen Plus.

2.6 Syngas mixing and upgrading

The syngas mixing section is the area that mixes and adjusts the syngas to a desired H_2/CO ratio or sends it to power generation. Additional unit operations that are present in this section are the WGS reactor and the ATR reactor, which are discussed next.

The purpose of the water gas shift reactor (WGSR) section is to upgrade syngas coming from the biomass gasifier which has a low H_2/CO ratio to a higher ratio of 2.01, since this syngas is destined for methanol and Fischer-Tropsch chemical production.^[16] The WGSR was modeled as a set of three adiabatic REQUIL reactors in series, which assumes chemical equilibrium using a 20°C approach temperature. The sequencing of reactors exploits the fast kinetics of the first two reactors, but utilizes the favourable low temperature equilibrium of the reaction system at the end.^[30] The low temperature reactor exploits the equilibrium moving more towards the products, namely hydrogen gas. Steam is added to the entrance of the first reactor such that a syngas H_2/CO ratio of 2.01 is obtained at the exit of the last reactor. A schematic of the WGSR section is shown below in Figure 5. Note that the flow rate of this section varies widely between simulation cases. In practice, the high temperature reaction takes place between 300 and 450°C over a $Fe_2O_3/Cr_2O_3/CuO$ catalyst. The low temperature reaction occurs over a $Cu/ZnO/Al_2O_3$ catalyst between 120 and 300°C. The intercooler temperature output settings chosen were about 327°C and 232°C for the first and second intercoolers, respectively. These are subject to optimization but the impacts of changes in temperature on the design and its performance are minimal.

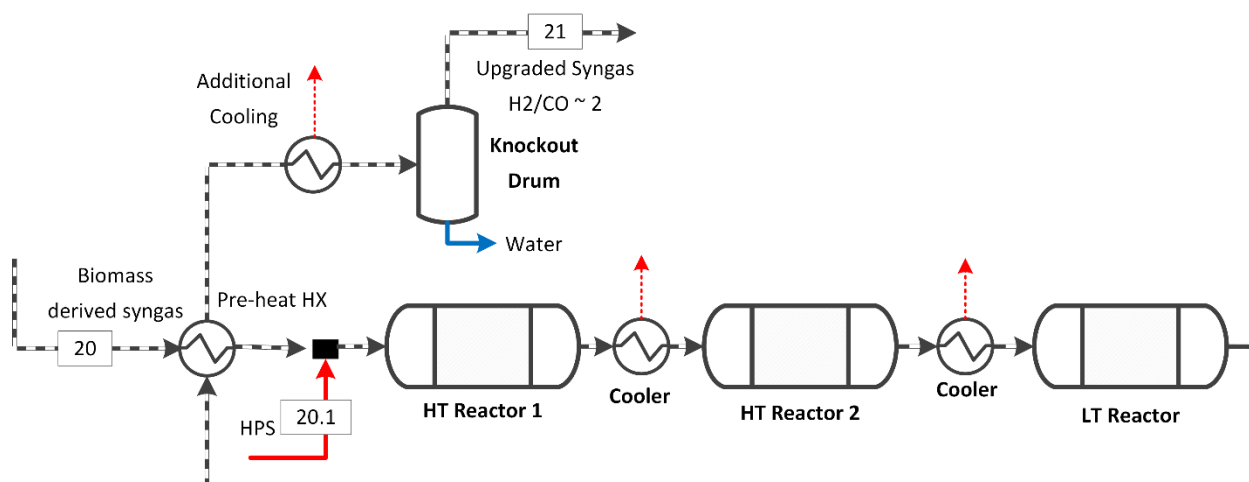


Figure 5. The Aspen Plus model of the WGS section.

For some cases, an ATR section is used to create hydrogen-rich syngas derived from natural gas, steam and oxygen (this is a separate reactor from the SMR integrated with the gasifier's radiant cooler). The hydrogen-rich syngas can be mixed with biomass-derived syngas for power or to increase the hydrogen content for fuels and chemical production. An outline of the model is shown in Figure 6. The system consists of a pre-reformer, the ATR, a system of heat exchangers, and a flash drum for water removal. The pre-reformer and the main reformer were modeled as adiabatic equilibrium reactors in Aspen Plus. The reactors operated at 30 bar due to the availability of natural gas at this pressure and the need for high pressure syngas downstream. The assumed pressure drop of the pre-reformer and main reformer were 0.4 bar and 0.6 bar, respectively.^[26] The purpose of the first reformer is to pre-reform the syngas and totally reform the largest hydrocarbons ($C_2 - C_4$), while the purpose of the second reformer is to oxidize a portion of the methane in the natural gas to provide the heat to drive the endothermic methane steam reforming reaction. The amount of high pressure steam that was added to each reformer was selected according to the methodology of Adams and Barton^[16] to prevent carbon deposition, provide adequate methane conversion, and avoid excessive steam use. The amount of oxygen added to the system was chosen so that the outlet temperature of the main reformer was 950°C. The pre-reformer inlet was preheated to 500°C and the main reformer inlet was preheated to 840°C.

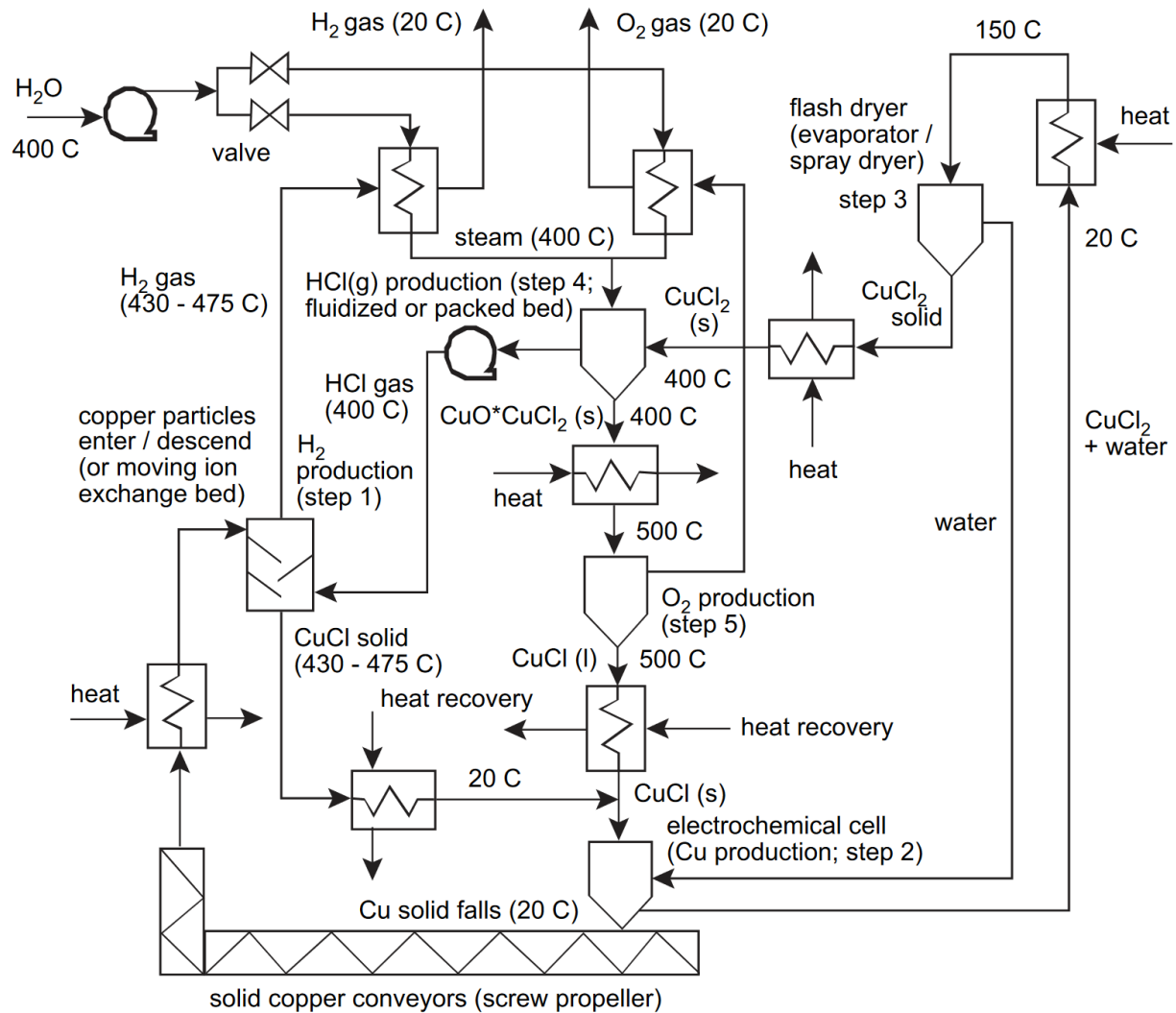


Figure 7. The Cu-Cl cycle, reprinted from Rosen^[34] with permission from Elsevier.

In this work, it is assumed that some of the heat from the CanDU SCWR is used for the heating step for Step 4 (via an intermediate loop with helium as the heat carrier), with the remainder of the SCWR heat used for power generation explicitly for electrochemical splitting (step 2) and the balance of the nuclear plant needs, as shown in Figure 8. For this work, we assume that no additional electric power comes from nuclear energy and the SCWR is sized only to produce the necessary hydrogen.

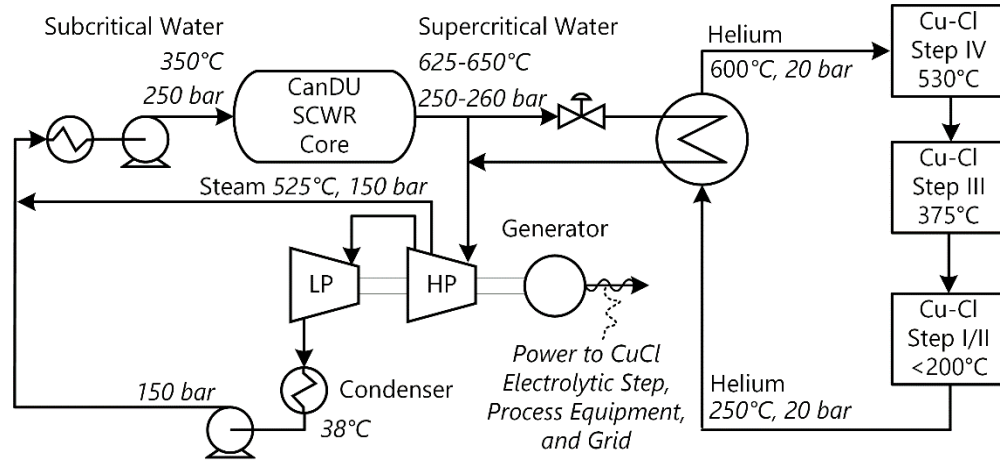


Figure 8. The CanDU SCWR reactor integrated with a Cu-Cl cycle, based on the original drawing in Tsvetkov.^[35]

It was assumed that the CuCl cycle acts as a stand-alone external utility, and the water required solved by mass balance. It was assumed that it took 145 MJ of thermal energy and 60.7 MJ of electric energy to generate 1 kg of hydrogen.^[31] However, assuming the thermal efficiency of the SCWR is 50%, a total of 266 MJ of thermal energy from the SCWR is required to generate 1 kg of H₂ in this process.^[32] The oxygen generated by the CuCl cycle is used to displace the oxygen generated by the ASU, making its size and energy consumption smaller. The outlet conditions of the O₂ and H₂ from the CuCl cycle are assumed to be 20°C and 10 bar.^[34] For details about the Cu-Cl process and how it can be integrated with a CanDU SCWR, the reader is referred to Rosen^[34] and Tsvetkov^[35] respectively.

Figure 9 shows the syngas upgrading section superstructure. The various stream split percentages, such as the amount of syngas used for liquid fuels production (and which kind of fuel) vs. power generation, the amount of diversion for the water gas shift section, and the amount of natural-gas derived syngas used for blending or for power are all design degrees of freedom. If both nuclear heat is used and FT is used, all of the hydrocracker H₂ needs in the FT section are met through stream 26.1.

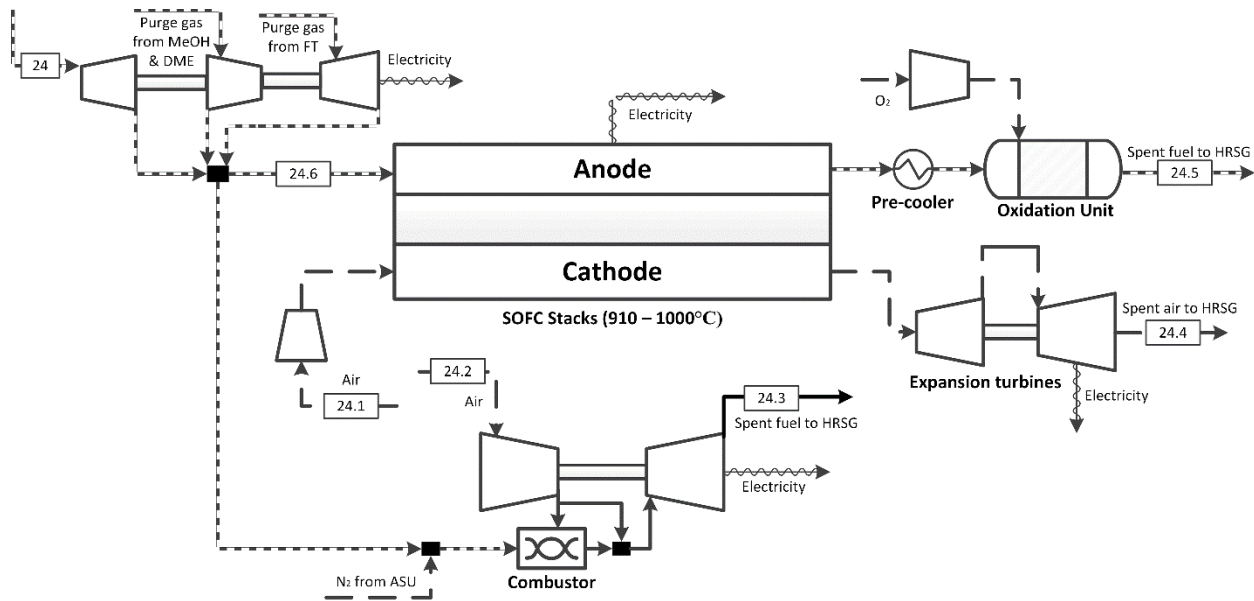


Figure 10. The power generation section superstructure. The O_2 feed for the SOFC post-oxidation unit is produced by the ASU.

The SOFCs are powered by syngas in the anode with ordinary air in the cathode, each at about 20 bar pressure. The CO and H_2 present in the feed is electrochemically oxidized directly into CO_2 and H_2O by reaction of oxygen ions which migrate from the cathode to the anode through the solid electrolyte barrier. This prevents N_2 from entering the fuel exhaust, thus allowing two separate outlet streams. The hot cathode exhaust is used for additional electricity in a Brayton cycle, and the anode exhaust, which still contains some CO and H_2 , is further oxidized catalytically using O_2 from the ASU. This results in a stream of only CO_2 and H_2O , which can be separated through a series of flash drums, thus facilitating low-energy CO_2 capture. The CO_2 is captured at high pressure (19-20 bar) and the water is recovered at high purity at atmospheric pressure. The captured CO_2 is further compressed in a compression and sequestration section described later.

The Aspen Plus model for the SOFC system was originally developed in previous works and fully described there.^[19, 26] The key assumed parameters are that the system achieves a voltage of 0.86V, has a DC to AC inversion efficiency of 96%, and that 5% of all energy released by oxidation in the SOFC is lost as waste heat. An integrated cooling system keeps temperatures in the 910 to 1030°C range, which is recovered in the HRSG. The post-anode catalytic oxidation system used stoichiometric air from the ASU with a boost compressor and was modelled assuming 99%

conversion of energy chemicals (H_2 , CO , CH_4 , methanol, ethanol, DME, and methyl formate) in an adiabatic RSTOIC block. The Aspen Plus model for the flash drum purification section is not shown in Figure 10 for brevity but is described fully in Adams and Barton^[19] and accounted for in the analysis.

The gas turbine in this work (also shown in Figure 10) was modeled using RGibbs and compressors/turbine blocks in Aspen Plus. The inlet pressure to the gas turbine was 21 bar, and 9% excess O_2 (in the form of air) was added to the gas turbine for combustion. A portion of this air stream was split and sent to mix with the combusted fuel to maintain a safe operating outlet combustion temperature.^[16, 24] In addition, waste N_2 was mixed from the ASU to dilute the incoming fuel stream and to achieve a lower heating value of $4.81\text{MJ}/\text{Nm}^3$.^[16] The electrical conversion was also assumed to be 100% efficient for the gas turbine^[24] while mechanical conversion used the values noted in Table 3. The spent fuel is then sent to the HRSG section for heat recovery.

2.8 Carbon dioxide removal from syngas

This section uses MDEA to remove CO_2 from syngas prior to use in the FT section. This step is needed because the FT catalyst can tolerate no more than 5% inert gas content in the feed,^[36] and other inert chemicals (such as N_2) are much harder to remove. In addition, much of the remaining H_2S left in the syngas is also absorbed along with the CO_2 . The feed to the CO_2 removal section is a mixture of blended syngas from upstream with recycle FT off-gases from downstream (including a recycle compressor).

This process was modeled in ProMax, utilizing the TSWEET kinetics property package, as shown in Figure 11. The CO_2 removal process uses a classic configuration containing a contacting absorption column and regenerative stripper column. The absorption column operates at high pressure (15 ideal stages / 45 actual trays – 38 bar pressure at the top and 39 bar bottom), while the stripper column operates at a relatively low pressure (10 ideal stages / 30 actual trays – 1.8 bar at the top and 2 bar bottom). In addition, low pressure steam is used to heat the bottom of the column and cooling water is used in all of the cooling blocks.

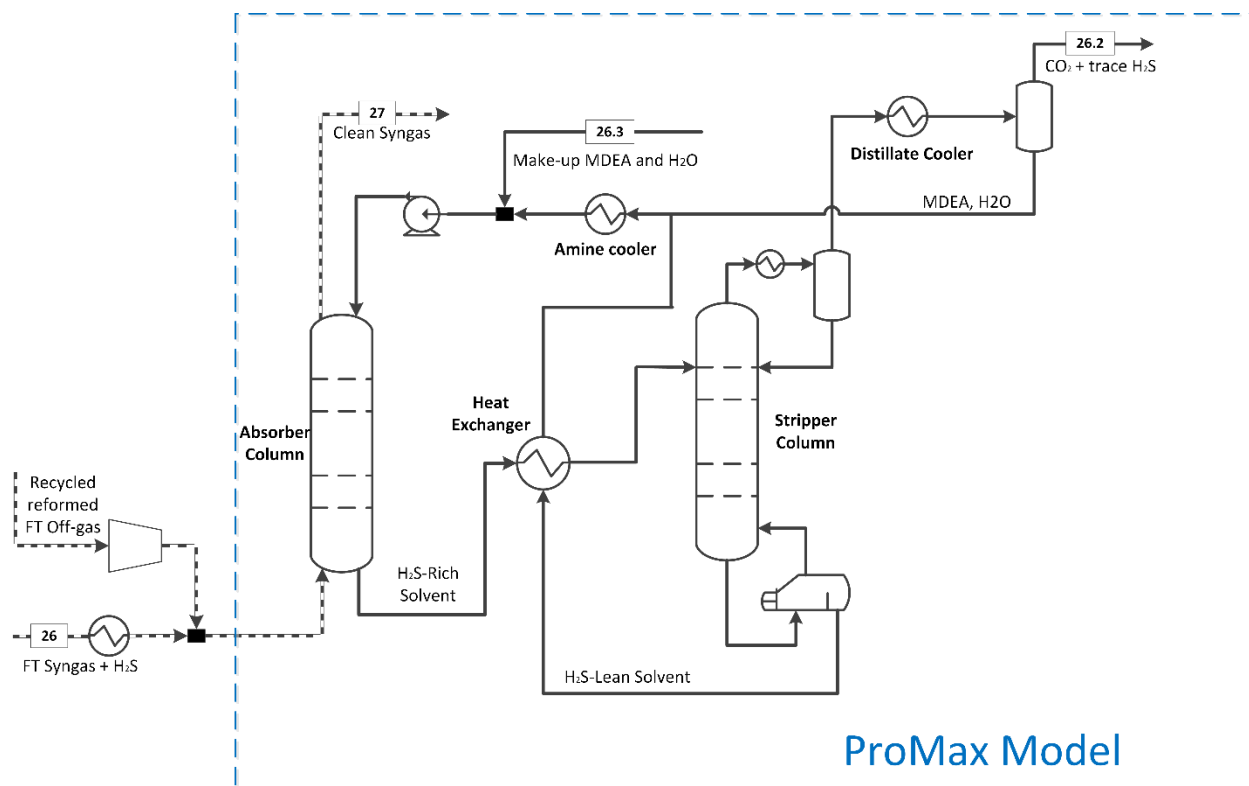


Figure 11. The section for removing CO₂ from syngas destined for liquid fuels production. The compressor and mixer are modelled in Aspen Plus, and the balance are modelled in ProMax.

An ROSSM was constructed from the ProMax model such that it could be incorporated into the Aspen Plus flowsheet using a combination of Calculator and SEP blocks, making execution fast within Aspen Plus. The ROSSM is suitable for use only in the range of CO₂ concentrations and syngas flow rates encountered in this study, and is not generalizable to other applications. It was found that a linear model was sufficient for predicting key performance parameters such as makeup solvent flow rates and heat exchanger duties, with higher order polynomials achieving little improvement. The model was trained with 55 simulation points (spaced evenly with just one independent variable, the flow rate of CO₂ in the feed stream) with 20 additional simulations used as the testing set. Each ProMax simulation was defined such that solvent flow rates were adjusted such that 90% of the CO₂ was removed from the syngas. The resulting model is described in detail in appendix Table A2. The linear ROSSM describes the ProMax model very accurately for key parameters such as heat exchanger duties. Although it is less accurate at predicting makeup

solvent flow rates (maximum 5% error), those flow rates have a very minor impact on the economics and so it is acceptable.

2.9 Fischer-Tropsch section

The FT section is shown in Figure 12. Upstream syngas with an H_2/CO ratio of 2 is sent to the FT cobalt-based reactor where it is pre-heated to 240°C and reacted at 36 bar to generate hydrocarbons with hydrocarbon up to 60. The model of Adams and Barton^[16] was used for this section which is described fully in that work and so is described here only briefly. The model for the FT reactor considers only straight alkyls, not branched, and for hydrocarbons pentane and higher, an Anderson-Schultz-Flory distribution with $\alpha=0.92$ and a CO conversion of 65% is assumed. Lower hydrocarbons have assumed product mixture concentrations as follows: CH_4 at 5 mol%, C_2H_4 at 0.05%, CO_2 , C_2H_6 , C_3H_8 , C_4H_{10} at 1%, and C_3H_6 and C_4H_8 at 2%. The model considers most of the hydrocarbons as separate chemicals but larger hydrocarbons above a carbon number of 31 use representative chemicals to represent a group (for example, C_{31} through C_{32} are modelled as $C_{32}H_{66}$).

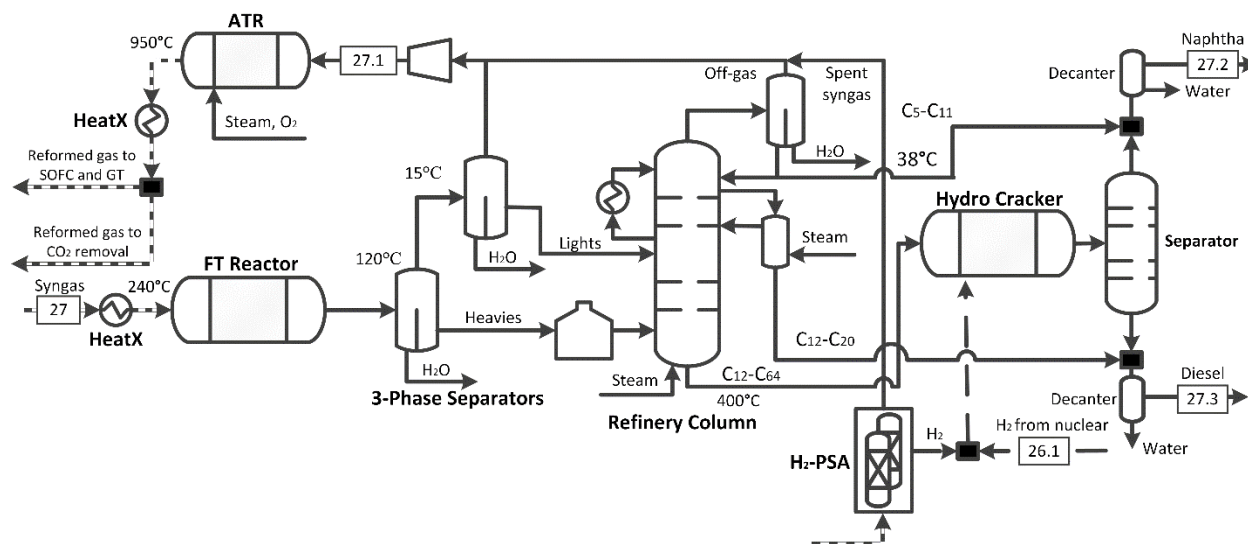


Figure 12. The model for the FT section of the superstructure.

Once the FT products exit the reactor, they are subsequently cooled by two 3-phase flash tanks, which separate water destined for water treatment into two groups - the lights (naphtha ($C_5 - C_{11}$)) and heavies ($C_{12} - C_{20}$). These are sent to the refinery column, while off-gasses are sent to an ATR

(which operates at 950°C and at an exit H₂/CO ratio of 2) in the FT section for reforming. The off-gasses are then either recycled back to the CO₂ removal section or sent to power generation as a decision variable. The light and heavy components then enter the refinery column which is modeled in Aspen Plus using the PetroFrac block. The column has 20 stages with a top pressure of 2.7 bar and a bottom pressure of 3.4 bar. The reboiler operates at 430°C and the condenser operates at 38°C. In addition, the following ASTM design specification for the tower was used: 95% vol: gasoline 170°C and diesel 340°C.

After the refinery column, the heavier hydrocarbons are sent to the hydrocracker where the carbon chains are broken into smaller chains for fuels production. Hydrogen is added to the hydrocracker either by pressure-swing absorption, where a portion of the FT feed has its hydrogen stripped from it for use in the hydrocracker as indicated in Figure 3.13, or by H₂ generated in the CuCl cycle if the nuclear option was chosen in the superstructure. The hydrocracker model uses a plug-flow kinetic model, with more details described in Adams and Barton^[16]. The separator following the hydrocracker was not modelled since it has a small impact on plant costs, and instead it is assumed that hydrocarbons C₁₁ and smaller leave through the top and heavier hydrocarbons leave through the bottoms. Similarly, the product decanters assume perfect water removal for simplicity.

2.10 Methanol and dimethyl ether synthesis

The methanol and DME section is shown in Figure 13. This section produces methanol and DME from H₂/CO = 2 syngas with two separate reaction pathways. The model for this section was adapted from the model developed by Khojestah Salkuyeh and Adams^[15] and the details are fully described in that work and so it is summarized here only briefly. The first step in this process is methanol synthesis over a Cu/ZnO/Al₂O₃ catalyst (with simultaneous water gas shift reaction) in a reactor. The reactor model uses the Aspen Plus plug flow reactor model with Langmuri Hinshelwood Hougen Watson (LHHW) kinetics.^[37] It considers the methanol synthesis reaction, the water gas shift reaction, and the formation of ethanol and methyl formate, and operates adiabatically with an exit temperature of 240°C.

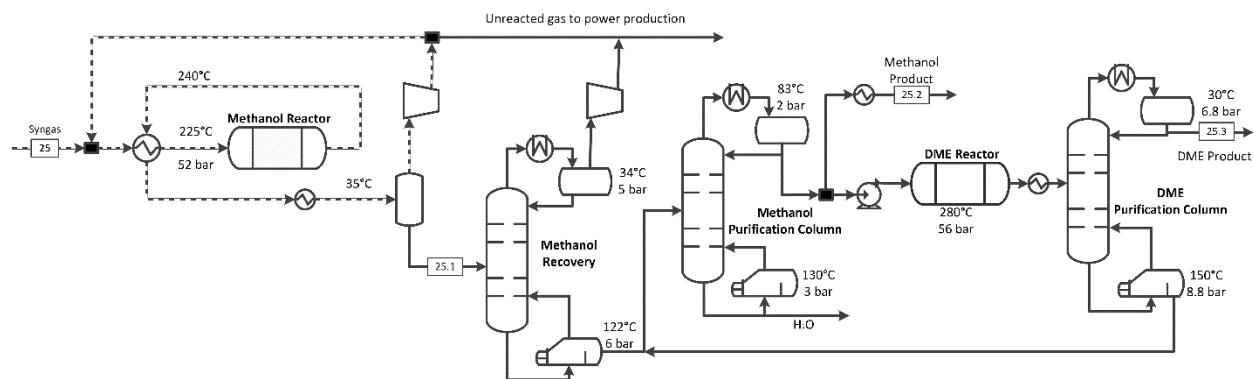


Figure 13. The model for the methanol and DME synthesis section of the superstructure.

The unreacted syngas is then cooled down to 35°C and is flashed in a flash drum (mostly unreacted gases such as N₂, CO and H₂). A portion of the off-gas is recycled back to the start of the reactor and the rest sent to the power generating section. After the liquid methanol exits the first drum, it is distilled in a methanol recovery unit, which acts as a second light gas removing column. This column was modeled using a RadFrac block in Aspen Plus with 20 equilibrium stages using the NRTL-RK property method. The off gases of the methanol recovery column are then sent to the power generating section. The methanol purification column then purifies the incoming methanol to 99.5% mol purity, with the bottom of the column being mostly water. This column was modeled as a RadFrac column using 40 equilibrium stages and the NRTL-RK property package. After the methanol purification column, a portion of the methanol is split for sale (a decision variable) and the remainder is sent to DME synthesis.

The portion of the methanol that is sent to DME synthesis is first pressurized to 56 bar and sent to a single-pass DME reactor operating at 280°C and 56 bar.^[24] The reaction takes place in the DME reactor over a γ -Al₂O₃ catalyst, considering the dehydration reaction kinetics of Bercic and Levic.^[38] DME is then recovered in the DME purification column, which is modeled using RadFrac with 30 equilibrium stages, utilizing the NRTL-RK package. The DME is purified to 99.5mol% at the top of the column and the bottom of the column is recycled back to the methanol purification column.

2.11 Heat recovery and steam generation

The purpose of the HRSG section is to take waste heat from the plant and generate various pressures of steam for additional power production and steam supply demands across the plant. There are three levels of steam used in this work: High Pressure (HP) (500°C, 50bar), Medium Pressure (MP) (300°C, 20bar), and Low Pressure (LP) (180°C, 5bar) steam. Various parts of the process utilize these different levels of steam, and steam demand outlets are made for each steam pressure based on plant demands. Minimum approach temperatures of 10°C are used when constructing the various heat exchangers across the plant.^[39] The excess steam that is not consumed by the plant is sent through 3 steam turbines, which generate additional power for the plant. In addition, boiler feed water heating and deaerating are taken into consideration when modeling the HRSG plant. The heat recovery section is shown in Figure 14.

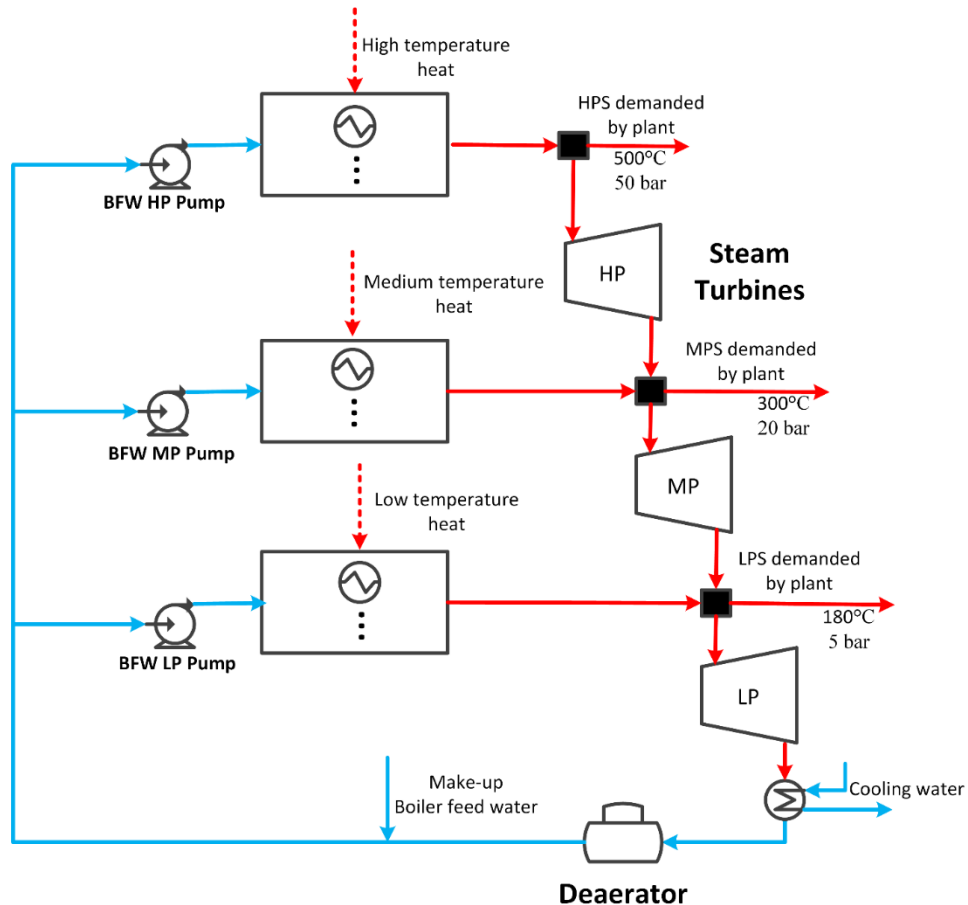


Figure 14: Model for the HRSG section of the plant.

This section focuses on compressing CO₂ from various parts of the plant and sequestering it at 153 bar pressure. This stage is particularly energy intensive as there are multiple cooling steps involved and large power demands from the multiple compressors that are involved. For this reason, this section is omitted for non-CCS cases. This section is modeled using the PSRK equation of state as it more accurately models the equilibrium of water and CO₂ in the liquid and gas phases at the relevant pressures of interest.^[19] The various captured CO₂ streams are mixed at different stages of the compression sequence depending on their available pressure levels. The multi-stage compression models in Aspen Plus used cooling water to cool the interstage compressor outlets to 30-80°C to both help with water removal (using flash drums) and to ensure compressor temperatures did not rise above 200°C. Once CO₂ has reached supercritical pressures, it is pumped to 153 bar for pipeline transport. The upstream CO₂ capture sections are designed to ensure that the purity of CO₂ is sufficient for most existing CO₂ pipelines.^[19] The process is shown in Figure 15.

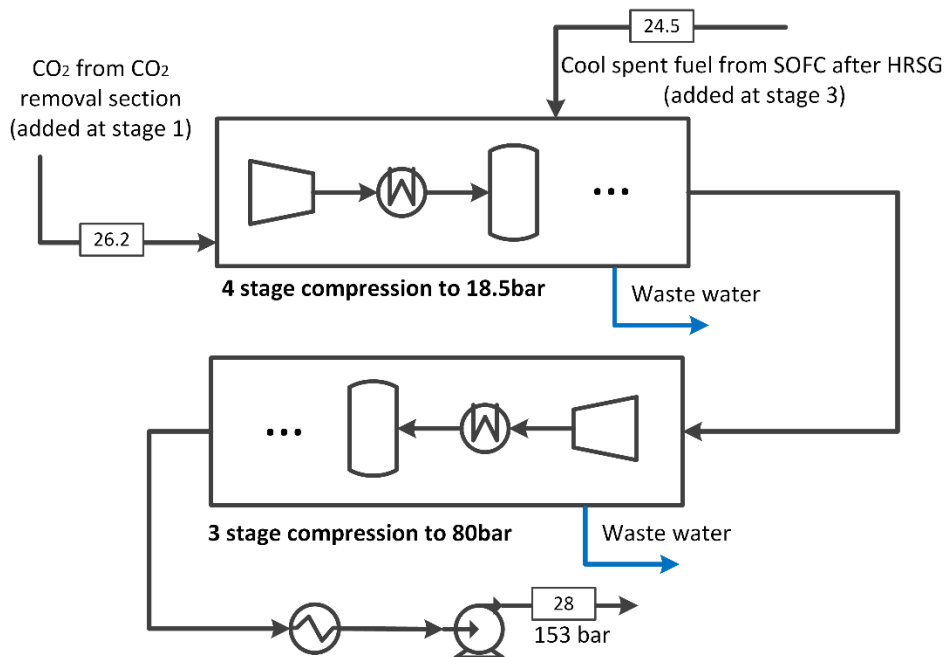


Figure 15: CO₂ compression section.

2.13 Cooling tower section

The cooling water section was modeled in this work as a two-stage equilibrium RadFrac column in Aspen Plus.^[40] External air was blown through the tower to remove the heat of the incoming

return cooling water ($\sim 50^{\circ}\text{C}$) from the plant. Some of the water escapes as water vapour through the top of the tower; as such, makeup cooling water is added to the plant return water, which is around 30°C . The incoming air is assumed to be 20°C . In addition to the cooling tower, there are other utilities that require extra cooling, so chilled water is used for these streams. The cooling water streams were modeled as utility streams with temperature inlet and outlet of $7^{\circ}\text{C} - 32^{\circ}\text{C}$.^[39] The model is summarized in Figure 16.

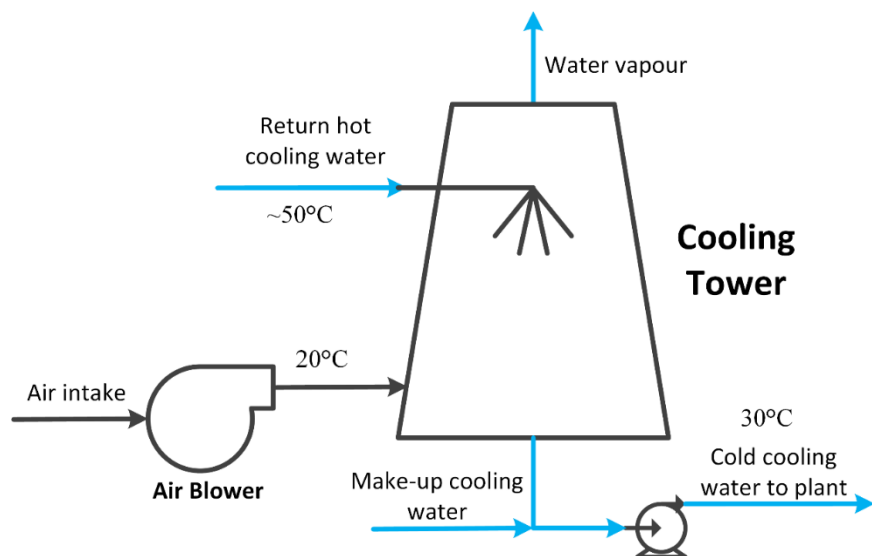


Figure 16. The model of the cooling tower section.

3. SIMULATION RESULTS

As a demonstration of model capabilities, two base case simulations were run for the two corresponding design cases shown in Table 1. The decision variables for these cases, such as how much syngas to divert to liquid fuels or power generation, and how much methanol to keep as a product and how much to use for DME synthesis, were all fixed to approximately the middle of their feasible ranges. This creates a sort of “average” plant which is suitable for a base case because it demonstrates all aspects of the superstructure at reasonably large sizes. It is certainly not optimal, but the optimal design will be very different depending on the objective function (i.e. environmental, economic, or both), market conditions, and business-related constraints. These optimality issues will be discussed in Part II of this work.

Sample stream conditions for Base Case 1.1 are shown in Table 4, which includes all of the advanced options (nuclear hydrogen production, integrated steam methane reforming and syngas cooling, and CO₂ capture and sequestration), and includes a mix of all possible products (SOFC-generated electricity, gas-turbine-generated electricity, FT liquids, methanol, and DME). Stream numbers in Table 4 correspond to the stream labels in Figures 2 through 16. In addition, a summary of key energy balance results is provided in Table 5. The thermal efficiency as reported in Table 5 is defined as follows:

$$\text{Thermal Efficiency (HHV)} = \frac{HHV_{DME} + HHV_{MeOH} + HHV_{Diesel} + HHV_{gasoline} + W_{elec}}{HHV_{biomass} + HHV_{naturalgas} + Q_{nuclearheat}}$$

Where W_{elec} is the net electric work (AC, grid quality) generated by the plant, $Q_{nuclearheat}$ is the amount heat collected from the nuclear reactor for CuCl process purposes (not the energy content of the uranium), and the HHV terms are the higher heating values of the fuels produced (DME, methanol, FT diesel and FT gasoline) and feedstocks as appropriate. The relative amount of electricity produced is also on an HHV basis and is defined as follows:

$$\text{Percentage of Output as Electricity} = \frac{W_{elec}}{W_{elec} + HHV_{DME} + HHV_{MeOH} + HHV_{Diesel} + HHV_{gasoline}}$$

The total direct GHG emissions reported in Table 5 are expressed in CO₂ emissions equivalents (CO₂e) using the standard International Panel on Climate Change 100-year metric.^[41] They include only the GHG emissions directly leaving the plant through plant exhaust, which are primarily CO₂ with trace amounts of CH₄. This includes the effects of creating all utilities necessary since they are included in the model (e.g. various steam pressures, electricity, cooling services). It does not take into account upstream and downstream GHG emissions associated with production, use, transportation, or storage of CO₂, which is instead discussed in Part II of this work in detail.

Table 4 (Continued).

[illegible]

Table 4 (Continued).

Stream ID	27-3	28
T (°C)	200	57
P (bar)	3	153
F (kmol/h)	41	3847
Vap. Frac	0	0
Mole Fractions (% unless otherwise noted)		
H ₂		0.2
CO		995 ppm
CO ₂	1 ppb	98.1
H ₂ O		7 ppm
Ar		0.3
O ₂		0.2
N ₂		1.1
H ₂ S		29 ppm
CH ₄		532 ppm
CH ₃ OH		572 ppb
C ₂ H ₅ OH		3 ppb
HCOOCH ₃		1 ppm
C ₂ to C ₅	496 ppb	
C ₆ to C ₁₁	3.4	
C ₁₂ to C ₂₀	90.8	

Table 5. Summary of mass and energy balance results for the two base case examples, assuming 365/24/7 operation at 100% capacity.

Case	1.1	1.2
Uses CCS?	Yes	Yes
Syngas Cooling	IR	RSC
<i>Energy Inputs (MW by HHV)</i>		
Wood Chips	550	550
Natural Gas	833	664
Nuclear Heat	117	117
<i>Total</i>	1500	1331
<i>Energy Outputs (MW by HHV or electricity)</i>		
Electricity	170	152
Diesel	103	86
Gasoline	46	39
Methanol	47	39
DME	360	303
<i>Total</i>	726	619
Thermal Efficiency (%HHV)	48.4%	46.5%
Carbon Efficiency (C in Products / C in Feedstock)	46.7%	44.0%
Direct GHG Emissions (tCO ₂ e/yr)	314,074	295,253
Captured CO ₂ (tCO ₂ e/yr)	1,236,501	1,171,601
Direct CO ₂ Emissions Per MJ _{HHV} products (kg/MJ _{HHV})	9.96	9.36

The results of Table 5 show that Case 1.2, which uses classic steam generation in the RSC, has a lower thermal efficiency by about 2 percentage points than using the integrated reformer, all else being equal. The power and work breakdown for these two cases is shown in Table 6. More power is produced in the high and medium pressure turbines in the HRSG in Case 1.2 because of the extra steam generation, and the total electric power produced in Case 1.2 as a percentage of the total energy output is also about 1 percentage point higher. However, the overall efficiency of Case 1.1 is higher because the additional liquid fuels that can be produced from the integrated reforming process more than makes up for this difference. This is expected because Case 1.1 makes better use of the exergy available in the RSC by making more liquid fuels instead of high pressure steam.

Table 6. Summary of power consumed or produced by unit the for two cases, in MW.

	Case	Case		Case	Case
	1.1	1.2		1.1	1.2
<i>Biomass Gasification</i>			<i>Cooling Towers</i>		
Biomass crushing	11.0	11.0	Air compressors	3.5	3.2
ASU	41.3	37.9	Water pump	8.3	7.6
Primary O ₂ booster (to 12.9 bar)	0.3	0.3	<i>Power Island</i>		
Secondary O ₂ booster (to 47 bar)	2.0	2.0	Gas turbine air compression	26.5	21.7
Quench water pump	0.2	0.2	Gas turbine power production	-67.1	-55.3
<i>Syngas Mixing and Upgrading</i>			SOFC cathode air compression.	47.8	41.6
O ₂ boost compression (to 30 bar)	1.0	1.0	FT off-gas expander	-0.1	-0.1
Syngas compressor (from IR)	1.4	N/A	MeOH off-gas expander	-0.1	-0.1
Syngas compressor (from ATR)	2.2	2.2	Syngas expander for SOFC anode	-0.7	-0.6
Syngas compressor (MeOH-bound)	2.8	2.5	SOFC stack power	-151.4	-131.2
<i>CO₂ Capture Sections</i>			O ₂ boost compressor	0.3	0.2
MDEA Section	0.3	0.3	Cathode exhaust turbine stage 1	-29.2	-25.4
FT of-gas recycle compressor	0.2	0.2	Cathode exhaust turbine stage 2	-19.8	-17.2
<i>CO₂ Compression Section</i>			<i>Heat Recovery and Steam Generation</i>		
Compression train 1 (to 19 bar)	4.8	4.6	Boiler feedwater pumping	0.7	0.7
Compression train 2 (to 80 bar)	4.5	4.2	High pressure gas turbine	-2.7	-5.4
Supercritical pumping to pipeline	0.9	0.9	Medium pressure gas turbine	-13.9	-15.3
<i>FT Synthesis Section</i>			Low pressure gas turbine	-48.2	-46.3
O ₂ boost compressor (to 40 bar)	0.3	0.2			
Distillation bottoms pump	0.0	0.0	GROSS POWER CONSUMPTION	163	145
Flash drum vapor product compr.	0.4	0.3	GROSS POWER PRODUCTION	333	297
Distillate off gas recycle compr.	1.0	0.8	NET POWER PRODUCTION	170	152
<i>Methanol Synthesis Section</i>					
Off-gas recycle compressor	1.1	1.0			
Methanol pump	0.2	0.1			

Note that it is not possible to make conclusions as to whether one design concept is “better” than the other in general because these base cases have not been optimized, nor have we defined economic or processing objectives. That will be explored in detail in a future work.

The largest consumers of power are the ASU, biomass crushing, and air compression for the power generation units, together comprising more than 77% of the parasitic load. Most of the remaining units are relatively small. The power surplus indicates that a greater percentage of syngas could be used for liquid fuels if desired and still have enough energy available to meet all process electricity and steam needs.

The contribution of the nuclear component is relatively small at roughly 8-9% of the total energy input. This indicates that need for hydrogen required for syngas upgrading for fuel production is relatively small. Although the nuclear component could increase in importance as more liquid fuels are produced, about 75% of the output is already liquid fuels in this example and so the nuclear hydrogen demand would not increase by more than roughly a third. In order to increase the potential contribution of the nuclear component, it may be beneficial to use additional nuclear heat for steam methane reforming in the ATR (if present) and/or instead of using the IR, as proposed by Khojastah and Adams.^[14]

The GHG emissions reductions potential using CCS is quite large, with about 80% of the CO₂ produced captured, in this example. For the CCS-enabled plants, the atmospheric emissions primarily come through gas turbine exhaust, since post-combustion capture is not considered due to its relative inefficiency.^[42] If only SOFCs were used, then the GHG emissions arising from power generation could approach trivially small amounts since even the off-gases from liquids productions can be used in the SOFC. In case 1.1, approximately 49 t/hr of carbon (atomic) enters the process via wood, and about 42 t/hr of carbon enters via natural gas. Of this, about 42 t/hr of C is recovered as a fuel product. This gives a carbon efficiency of approximately 46.7%, which is defined as the percentage of carbon in the feed that ends up in a useful product (instead of captured or emitted CO₂ or other GHGs). This is quite good considering that more than half of the carbon source is biogenic, although a detailed life cycle analysis is left for future work. Case

1.2 has a lower carbon efficiency because it has a lower percentage of liquid fuels produced. For the same reason, Case 1.2 has a lower direct CO₂ emissions per MJ of products produced, since CO₂ capture happens mostly as a result of power production as opposed to liquid fuel production. Neither metric indicates that Case 1.2 is any more or less environmentally friendly than Case 1.1 because the product portfolios are different. That will be determined in a future work by considering a complete life cycle analysis of optimized processes for specific business objectives.

4. CONCLUSIONS

Two new biomass, gas, and nuclear-to-liquids polygeneration process superstructures were presented in this work, each using different levels of advanced technologies. The nuclear component is primarily integrated through syngas upgrading using hydrogen produced via the CuCl cycle, and is particularly suitable for next generation Canadian nuclear reactor designs such as the CanDU SCWR. Ontario-grown cedar wood chips are used as one of the key feedstocks in conjunction with conventional pipeline natural gas. The process models have been provided as supplementary material so that they can be used by others for planning and design purposes.

The proposed superstructures are suitable for the co-production of electricity and various liquid fuels, and can be modified to suit whatever product portfolio is of most interest to the end user. Although there are various strengths and weaknesses to each of the different process types, the key difference is that the integrated reforming strategy uses the available heat of the RSC to make a larger percentage of higher value products (liquid fuels) than electricity, as compared to a classic steam generation strategy. However, the key differences in value between the processes are expected to be rooted in their environmental and economic properties, which are highly dependent on market conditions, public policy, and upstream and downstream end use supply chains. These issues are addressed in Part II of this work, which will use an optimization-based analysis that factors in capital and operating cost estimates, profitability analyses, cradle-to-grave life cycle analyses, and carbon taxes to make conclusions about which process designs are best suited for Ontario in different market conditions.

ACKNOWLEDGMENTS

This work was funded by contributions from an NSERC Canadian Graduate Scholarship, an Ontario Graduate Scholarship, and an Ontario Early Researcher Award (ER13-09-213).

APPENDIX

Table A1. ROSSM parameters for the integrated reformer model described in eq. (1) in section 2.3. The maximum absolute error is defined as point with the highest difference between the predicted and actual values of Z_i divided by the actual value, for the 80 points explored. The model is only valid within the range of $506.9 \leq F_{NG} \leq 753.5$ (MW) and $2.6 \leq R_{S:C} \leq 4.0$, with $\overline{F_{NG}} = 637.329$ MW and $\overline{R_{S:C}} = 3.293$.

Model Variable (i)	Z_1	Z_2	Z_3	Z_4	Z_5
Description	Required radiant cooling duty	CH ₄ conversion	H ₂ O conversion	Tube side exit Temperature	Tube side pressure drop
Units of Z_i (and $a_{j,i}$)	MW	unitless	unitless	°K	bar
$a_{1,i}$	5.726	1.068	0.864	1512	-14.815
$a_{2,i}$	32.529	-0.679	-0.231	-362.9	21.06
$a_{3,i}$	10.417	0.257	-0.571	-86.65	17.68
$a_{4,i}$	-9.871	0.144	0.027	110.4	-7.113
$a_{5,i}$	-2.601	-0.062	0.145	28.44	-4.098
$a_{6,i}$	2.336	0.030	0.096	-72.49	-18.06
R^2 of training data	1.00	1.00	1.00	1.00	1.00
R^2 of testing data	1.00	0.99	1.00	1.00	0.998
Max abs error	0.04%	0.14%	0.15%	0.03%	0.01%

Table A2. ROSSM model for the syngas CO₂ removal section described in section 2.8. The model is only valid within the range of $620.6025 \leq F_{CO_2} \leq 1033.75$ (kmol/hr) where F_{CO_2} is the inlet flow rates of the CO₂ contained within the syngas feed for a syngas feed typical of FT synthesis applications and scales, with the normalization factors of $\overline{F_{CO_2}} = 827.47$ kmol/hr. The model has the form: $Z_i = a_{1,i} + a_{2,i} \frac{F_{CO_2}}{\overline{F_{CO_2}}}$

Model Variable (i)	Z_1	Z_2	Z_3	Z_4	Z_5	Z_6	Z_7
Description	MDEA makeup	H ₂ O makeup	Pump power	Reboiler Duty	Condenser Duty	Distillate Cooler	Amine Cooler
Units of Z_i (and $a_{j,i}$)	kmol/hr	kmol/hr	kW	kW	kW	kW	kW
$a_{1,i}$	5.595x10 ⁻⁴	-1.235	3.099	-117.9	0.581	14.64	-74.48
$a_{2,i}$	6.709x10 ⁻³	40.92	425	15950	128.9	3220	7040
R^2 of training data	0.843	0.963	1	1	1	1	1
R^2 of testing data	0.812	0.900	0.997	0.998	0.999	0.999	0.991
Max abs error	5.0%	5.0%	0.7%	0.6%	0.4%	0.4%	1.1%

ABBREVIATIONS

ASU	air separation unit
ATR	autothermal reforming
BGNTL	biomass-gas-and-nuclear-to-liquids
BGTL	biomass-and-gas-to-liquids
CanDU	Canadian deuterium-uranium
CCS	carbon capture and sequestration
CO ₂ e	carbon dioxide emissions equivalents
DME	dimethyl ether
FT	Fischer-Tropsch
GHG	greenhouse gas
GT	gas turbine
HHV	higher heating value
HPS	high pressure steam
HRSG	heat recovery and steam generation
IR	integrated reformer
MDEA	Methyldiethanolamine
MeOH	methanol
RSC	radiant syngas cooler
SCWR	supercritical water reactor
SMR	steam methane reformer / steam methane reforming
SOFC	solid oxide fuel cell
t	(metric) tonne = 1000 kg
WGS	water gas shift

REFERENCES

1. Government of Ontario. Ontario's Five Year Climate Change Action Plan 2016-2020 (p86). Accessed Aug 2017.
http://www.applications.ene.gov.on.ca/ccap/products/CCAP_ENGLISH.pdf
2. Ontario Ministry of Energy. Ontario's Long Term Energy Plan. ISBN 978-1-4606-3187-4 (2013)

3. Environment and Climate Change Canada. Pan-Canadian Approach to Pricing Carbon Pollution. October 3, (2016). Government web site. Accessed Aug 2017. Accessible at <https://www.canada.ca/en/environment-climate-change/news/2016/10/canadian-approach-pricing-carbon-pollution.html>
4. Environment and Climate Change Canada. Technical Paper on the Federal Carbon Pricing Backstop. June 9, (2017). ISBN 978-0-660-08506-7.
5. Ontario Energy Board. Ontario's System-Wide Electricity Mix: 2016 Data (August 14, 2017). Accessible at https://www.oeb.ca/sites/default/files/2016_Supply_Mix_Data.pdf
6. Environmental Commissioner of Ontario. Facing Climate Change: Greenhouse Gas Progress Report, Chapter 2: Ontario's Carbon Footprint – Where are we now? (Nov 22, 2016). Accessible at <https://eco.on.ca/reports/2016-facing-climate-change/>
7. D.B. Levin, H. Zhu H, M. Beland, N. Cicek, B.E. Holbein, *Biores. Technol.* **2007**, 98, 654.
8. S. Krigstin, S. Wetzel, W. Mabey, S. Stadnyk, *Forest. Chron.* **2016**, 92, 189.
9. R. Levin, S. Krigstin, S. Wetzel, *Forest. Chron.*, **2011**, 87, 33.
10. World Nuclear Association. Uranium in Canada. (July 2017). Accessed September 2017. Accessible at <http://www.world-nuclear.org/information-library/country-profiles/countries-a-f/canada-uranium.aspx>
11. M. Naidin, S. Mokry, F. Baig, Y. Gospodinov, Y. Zirn, I. Pioro, G. Naterer, *J. Eng. Gas Turb. Power*, **2009**, 131, 12901.
12. G.F. Naterer, I. Dincer, C. Zamfirescu. Hydrogen Production from Nuclear Energy. Springer: London **2013**.
13. L. Hosenzade, T.A. Adams II, *Int. J. Hydrogen Energy* **2017**, doi: 10.1016/j.ijhydene.2017.08.031.
14. Y. Khojestah Salkuyeh, T.A. Adams II. *Energy Conversion Management* **2013**, 74, 492.
15. Y. Khojestah Salkuyeh, T.A. Adams II. *Energy Conversion Management* **2014**, 88, 411.
16. T.A. Adams II, P.I. Barton, *Fuel Process. Technol.* **2011**, 92, 639.
17. T.A. Adams II J.H. Ghouse, *Current Opinion Chem. Eng.* **2015**, 10, 87.
18. J.H. Ghouse, D. Seepersad, T.A. Adams II. *Fuel Process. Technol.* **2015**, 138, 378.
19. T.A. Adams II, P.I. Barton, *AIChE J.* **2010**, 56, 3120.

20. D. Hewson, A. Oo, K.J. Albion, A. Keir. Biomass residuals study for OPG repowering program. Report of The University of Western Ontario Research & Development Park, Sarnia-Lambton Campus (2011). Accessible at <http://www.canadiancleanpowercoalition.com/pdf/BM22%20-%20Biomass%20Residuals%20Study%20for%20OPG%20Repowering%20Program.pdf>
21. L. Zhang, Y. Ninomiya, Q. Wang, T. Yamashita, *Fuel* **2011**, 90, 77.
22. A. Van der Drift, A. Boerrigter, H. Coda, B. Cieplik, M.K. Hemmes, K. Van Ree, H. J. Veringa. Entrained flow gasification of biomass. Report ECN-C--04-0.39 of Energieonderzoek Centrum Nederland, Revision A (April 2004). Accessible at <https://www.ecn.nl/docs/library/report/2004/c04039.pdf>
23. R.P. Field, R. Brasington, *Ind. Eng. Chem. Res.* **2011**, 50, 11306.
24. L.R. Clausen, B. Elmegaard, N. Houbak, *Energy* **2010**, 35, 4831.
25. J.H. Ghouse, T.A. Adams II, *Int. J. Hydrogen Energy* **2013**, 38, 9984.
26. T.A. Adams II, P.I. Barton, *J. Power Sources* **2010**, 195, 1971.
27. T.A. Adams II, Y. Salkuyeh Khojestah, J. Nease. Process and simulations for solvent-based CO₂ capture and syngas cleanup. In: Reactor and Process Design In Sustainable Energy Technology, Elsevier: Amsterdam **2014**, pp 163-231.
28. D.H. Mackenzie, F.C. Prambil, C.A. Daniels, J.A. Bullin, *Energy Progress* **1987**, 7, 31.
29. C. Okoli, T.A. Adams II, *Ind. Eng. Chem. Res.* **2014**, 53, 11427.
30. T.A. Adams II, P.I. Barton, *Int. J. Hydrogen Energy* **2009**, 34, 8877.
31. M.S. Ferrandon, M.A. Lewis, D.F. Tatterson, R.V. Nankanic, M. Kumarc, L.W. Wedgewood, C. Nische. The hybrid Cu-Cl thermochemical cycle. *NHA annual hydrogen conference, Sacramento, CA*, 10:3310-3326 (2008).
32. G.F. Naterer, S. Suppia, L. Stolberg, M. Lewis, M. Ferrandon, Z. Wang, J. Avsec, *Int. J. Hydrogen Energy* **2011**, 36, 15486.
33. Z.L. Wang, G.F. Naterer, K.S. Gabriel, R. Gravelsins, V.N. Daggupati, *Int. J. Hydrogen Energy* **2010**, 35, 4820.
34. M.A. Rosen, *Energy* **2010**, 35, 1068.
35. P.V. Tsvetkov. Nuclear power deployment, operation, and sustainability. Rejeka, Croatia: InTech. **2010**

36. C.N. Hamelinck, A.P.C. Faaij, H. den Uil, H. Boerrigter, *Energy* **2004**, 9, 1743.
37. K.V. Bussche, G.H. Froment, *J. Catalysis* **1996**, 161, 1.
38. G. Bercic, J. Levec, *Ind. Eng. Chem. Res.* **1993**, 32, 2479.
39. W.D. Seider, J.D. Seader, D.R. Lewin, S. Widago. *Product and Process Design Principles: Synthesis, Analysis and Design* (3rd Ed). Hoboken, NJ: Wiley **2008**.
40. J.A. Queiroz, V.M.S. Rodrigues, H.A. Matos, F.G. Martins, *Energy Conversion Manage.* **2012**, 64, 43.
41. International Panel on Climate Change. Contribution of Working Group I to the Fifth Assessment Report of the Intergovernmental Panel on Climate Change. *Climate Change 2013: The Physical Science Basis*; T.F. Stocker, D. Qin, G.-K. Plattner, M. Tignor, K.S. Allen, J. Boschung, A. Nauels, Y. Xia, V. Bex, P.M. Midgley, Eds.; Cambridge University Press: Cambridge, UK; New York, NY, USA (2013); 1535p.
42. T.A. Adams II, L. Hoseinzade, P.B. Madabhushi, I.J. Okeke, *Processes* **2017**, 5, 44.